Revisit the anomalous bending elasticity of sharply bent DNA

Peiwen Cong,[1,2] Liang Dai,[3,4] Hu Chen,[5] Johan R. C. van der Maarel,[3,4] Patrick S. Doyle,[4,6] and Jie Yan[2,3,4,7,*]

[1] *Computation and Systems Biology, Singapore-MIT Alliance, Singapore 117576, Singapore*

[2] *Mechanobiology Institute, National University of Singapore, Singapore 117411, Singapore*

[3] *Department of Physics, National University of Singapore, Singapore 117551, Singapore*

[4] *BioSystems and Micromechanics, Singapore-MIT Alliance for Research and Technology Centre, Singapore 138602, Singapore*

[5] *Department of Physics, Xiamen University, Xiamen, 361005, China*

[6] *Department of Chemical Engineering, Massachusetts Institute of Technology, Cambridge, Massachusetts 02139, USA*

[7] *Centre for BioImaging Sciences, National University of Singapore, Singapore 117557, Singapore*

Abstract

Several recent experiments have suggested that sharply bent DNA has a surprisingly high bending flexibility, but the cause is poorly understood. It has been demonstrated that excitation of flexible defects can explain the results; while whether such defects can be excited under the level of DNA bending in those experiments has remained unclear and been debated. Interestingly, due to experimental design DNA contained pre-existing nicks in nearly all those experiments, while the potential effect of nicks have never been considered. Here, using full-atom molecular dynamics (MD) simulations, we show that nicks promote DNA basepair disruption at the nicked sites which drastically reduced DNA bending energy. In the absence of nicks, basepair disruption can also occur, but it requires a higher level of DNA bending. Overall, our results challenge the interpretations of previous sharp DNA bending experiments and highlight that the micromechanics of sharply bent DNA still remains an open question.

* Email address: phyyj@nus.edu.sg

I. INTRODUCTION

Many cellular processes such as DNA packaging and gene transcription require sharp DNA bending [1, 2]. Thus, knowledge of the mechanics of sharply bent DNA is critical to understand them. DNA is often modeled as a thickless polymer which is described by a spatial curve in 3-dimension. Non-sharply bent DNA has been reported to follow the worm-like chain (WLC) polymer model [3]. In WLC polymer model, for a short DNA, the bending energy is described by $\beta E(\theta; A) = (A/2L)\left(\hat{t}' - \hat{t}\right)^2 = (A/L)(1 - \cos\theta)$, where A is the bending persistence length of DNA. Here $\beta = 1/k_{\rm B}T$ scales energy into units of $k_{\rm B}T$, $L \ll A$ is the DNA contour length, $\hat{t}$, $\hat{t}'$ are tangent vectors at two DNA ends, and θ is the bending angle of DNA. The bending rigidity of B-form DNA has been experimentally determined to be $A \approx 50$ nm [4–7], which is further related to the Young's modulus Y of elastic rod through the relation $A = \beta Y I$. Here $I = \pi R^4/4$ is the DNA area moments of inertia, while R is its radius.

Mechanical anomaly of sharply bent DNA was reported in several recent experiments. Spontaneous probabilities of looping ~ 100 bp DNA into minicircles were reported several orders of magnitude larger than the WLC prediction [8, 9]. The level of DNA bending in such DNA minicircles is biologically important as it is similar to that involved in DNA wrapping around nucleosomes [10, 11]. In a typical DNA looping probability measurements, DNA looping is assisted by annealing of two short complementary single-stranded DNA (ssDNA) oligomers at the two double-stranded DNA (dsDNA) ends. The annealing is a necessary step for the subsequent chemical ligation to determine the looping probability [12]. As a result, in such experiments, two nicks exist right after annealing.

The interpretation of the experiments was based on equilibration between the nicked DNA minicircle and unlooped linear DNA [4], which can be validated in experiments. It also relied on a critical assumption that at the nicks the DNA bending elasticity is identical to that of the B-form DNA, meaning that the two DNA cohesive ends are in parallel and matching twist when they meet. This assumption was validated in many DNA looping experiments for > 200 bp DNA which reported DNA bending persistence length similar to that obtained in single-DNA stretching experiment [8, 12, 13]. However, it was never tested at the level of bending in ~ 100 bp DNA minicircles.

Mechanical anomaly of sharply bent DNA was also reported in other types of experiments

by actively bending short dsDNA fragments using ssDNA oligomers connecting the two dsDNA ends [14–16]. In some of these experiments, the dsDNA fragments also contained a nick in the middle [15, 16]. The interpretation of these experiments was based on an assumption that strand-separation does not occur at the ssDNA/dsDNA boundary. In the case of DNA containing nick, it additionally assumed that the nick does not affect the local mechanical properties of DNA compared to B-form DNA.

Assuming the nicks do not affect the local mechanical properties of DNA compared to B-form DNA, the above reported mechanical anomaly can be explained by breakdown of the WLC polymer model due to potential excitation of DNA structural defects when DNA is sharply bent. Indeed, it has been theoretically demonstrated that excitation of flexible mechanical defects under bending constraint through DNA melting or kinking could explain these results [17–19]. This possibility was in part supported by an experiment reporting that covalently closed $63-65$ bp DNA minicircles without nicks could be digested by the BAL-31 nuclease [20, 21], indicating ssDNA generated in these DNA minicircles. However, similar experiments revealed that BAL-31 nuclease could not digest DNA minicircles with a size of interest (~ 100 bp). Therefore, up to date no direct evidence demonstrating mechanical defects excited in ~ 100 bp DNA minicircles has been reported.

An alternative possibility, which has not been considered in previous explanations to the experiments, is that the pre-existing nicks in those experiments may become a "hotspot" for mechanical defect excitation. In this scenario, under weak bending condition, the two adjacent basepairs straddling the nick are stacked such that DNA remains in a B-form helical conformation and has a similar bending elasticity to B-DNA. However, at higher bending constraint, the nicked site might develop structural changes easier than nick-free B-DNA that in turn relaxes the overall DNA bending energy, resulting in the observed mechanical anomaly. This picture also implies that defect excitation would not occur in the nick-free region of DNA due to the relaxed bending in such region.

Motivated by this previously unexplored possibility, in this work, we carried out full-atom molecular dynamics (MD) simulation to investigate the mechanical responses of short dsDNA fragments (20 bp) under compressive load in the presence and absence of a nick in the DNA (see Appendix A for details on DNA constructs and MD simulations). We found that during sharp DNA bending a pre-existing nick could indeed facilitate flexible defect excitation at the nicked site. Our results also reveal that the nick-dependent defect excitation is sensitive

to temperature. Based on these results, we suggest that the previously reported mechanical anomaly of sharply bent DNA is likely a result of nick-dependent flexible defect excitation rather than an intrinsic mechanical response of B-form DNA.

II. RESULTS

A. DNA bending responses under weak and strong spring constraints

A 20 bp DNA segment is forced to bend by a spring with zero equilibrium length connected to the 2^{nd} and 19^{th} basepairs of the DNA (see Supplemental Fig. 1 [22] for DNA initial structure). 280 equilibrated DNA conformations were obtained in 14 independent simulations under various spring constraints in the range of $\kappa \in (8.0, 85.0)$ pN/nm taking from $50-70$ ns with 1 ns interval (Fig. 1). The distance d between the center-of-mass of the atom groups of the two connecting bases was monitored. And, in each basepair the inter-distances of atoms involved in hydrogen bonds formation, $h_{i,j}$, where i denotes the basepair index and j denotes the j^{th} hydrogen bond, were also monitored.

Two representative conformation snapshots at $t = 60$ ns during simulations confined by a weaker spring ($\kappa = 16.6$ pN/nm) and a stronger spring ($\kappa = 28.2$ pN/nm) reveal total different bending responses [Fig. 2(a) and 2(c)]. The DNA under the constraint of the stronger spring assumes a much more severely bent conformation than that under the weaker spring, which contains disrupted basepairs marked in the red shadowed area. The 280 DNA backbone conformations in the last 20 ns (*i.e.*, $50-70$ ns) obtained under various spring constraints κ in the range of $8.3-83.0$ pN/nm can be classified into two distinctive groups based on the level of bending (Fig. 1). In the weakly bent group obtained at $\kappa < 20.0$ pN/nm, the end-to-end distances of DNA are longer than that of the initial DNA (red line), indicating a balance between the spring elasticity and DNA bending elasticity which relax DNA to a more straight conformation. In the sharply bent group obtained at $\kappa > 25.0$ pN/nm, the end-to-end distances are significantly shorter than that of the initial DNA, indicating that the strong springs out-compete the DNA bending elasticity and force it to collapse till the two ends physically collide into each other, which is accompanied with disruptions of DNA basepairs [*e.g.*, the shadowed region in Fig. 2(c)].

We quantified the weakly bent DNA under $\kappa = 16.6$ pN/nm for its structural details.

The final value of $\langle d \rangle$, which was averaged over the last 20 ns data out of 70 ns simulation, is ~ 4.65 nm, which is slightly longer than the initial value $d_{\rm ini} \approx 4.20$ nm indicating the tendency of DNA to relax to a more straight conformation. It is still slightly shorter than the contour length of ~ 5.43 nm, indicating a weakly bent conformation due to this spring constraint. The minimal and maximal hydrogen bond lengths in each basepair averaged in the last 20 ns, $\langle \min(h_{i,j}) \rangle$ and $\langle \max(h_{i,j}) \rangle$ completely overlaps with those of control ($\kappa = 0$ pN/nm), indicating that the weakly bent DNA remained intact throughout 70 ns simulation [Fig. 2(b)]. The hydrogen bond length fluctuates within $0.26 - 0.33$ nm and its average value ~ 0.30 nm is consistent with that in crystal structures [23]. Hereafter, a basepair is considered as Watson-Crick basepair when all its hydrogen bond lengths are < 0.33 nm.

On the other hand, the B-DNA became unstable when $\kappa > 25.0$ pN/nm, resulting in sharply bent DNA conformations with a very short final $\langle d \rangle < 2.3$ nm (see Supplemental Fig. 2 [22]). Considering volume exclusion, it means that two DNA ends distance away from one another by only a DNA diameter. Such sharp DNA bending is accompanied with disruption of DNA basepairs. For one example, the conformation snapshot at 60 ns of a simulation with $\kappa = 28.2$ pN/nm containing a localized sharp bend near the middle of the DNA [Fig. 2(c)]. The $\langle \min(h_{i,j}) \rangle$ and $\langle \max(h_{i,j}) \rangle$ profiles of this sharply bent DNA [Fig. 2(d)] clearly indicate that the $11^{\rm th} - 13^{\rm th}$ basepairs are disrupted.

B. Basepair disruption results in localized sharp DNA bending

In order to analyze the influence of local DNA basepair disruption in sharply bent DNA on the overall DNA shapes, we calculated the bending angle between the intact $10^{\rm th}$ and $14^{\rm th}$ basepairs, which straddles the disrupted region, through $\theta_{10,14} = \cos^{-1}(\hat{z}_{10} \cdot \hat{z}_{14})$ for the DNA bent under $\kappa = 28.2$ pN/nm. Here $\hat{z}_i$ describes the normal direction of the $i^{\rm th}$ basepair (see Appendix B and Fig. 7). The first row in Fig. 3 shows that evolution of $\theta_{10,14}$ (black) from initial $\sim 40^\circ$ toward larger bending angle began immediately after the simulation started. Saturated local bending was reached within 10 ns, and remained at a high bending level of $\sim 160^\circ$ till the end.

For comparison, the bending angle evolutions of two unaffected regions of the same length, $\theta_{6,10}$ (cyan) and $\theta_{14,18}$ (orange), were plotted. Synchronized with DNA kink formation of $\theta_{10,14}$, their bending angles were relaxed from initial $\sim 40^\circ$ to lower values of $\sim 30^\circ$ and

$\sim 10^\circ$ within 10 ns, respectively, and remained at these low bending levels till the end. These results indicate the kink formation of $\theta_{10,14}$ relaxed the rest of the DNA to a more straight conformation.

We further examined the correlation between the localized kink formation and the disruption of the basepairs. Time traces of $h_{i,j}$ for the three affected `AT` basepairs $i = 11, 12, 13$ are shown in rows $2-4$ of Fig. 3. The results reveal that the 11^{th} basepair remained intact in the first ~ 48 ns, then was disrupted between ~ 48 and ~ 56 ns. After ~ 56 ns, it fluctuated between disrupted and intact states. The 12^{th} and 13^{th} basepairs opened up within 10 ns, then remained disrupted till the end. Clearly, DNA kink formation and disruptions of these basepairs are highly correlated; hence we conclude that basepair disruption caused kink development.

Similar localized kink development was observed in all twelve independent simulations using $\kappa > 25.0$ pN/nm, accompanied with basepair disruptions at the kinked locations. They mainly located around the same region near the center, likely due to high curvature at the center under our bending geometry (see Appendix C for details on central location of defects).

C. DNA conformational free energy and force distance curves

In order to understand the mechanics of DNA under bending, we calculated the DNA conformational free energy as a function of d and force required to maintain d using umbrella sampling.

Briefly, a series of springs indexed by m, each with a finite equilibrium length of l_m and fixed spring constant $\kappa_{\text{u}} = 248.9$ pN/nm, were used to induce DNA bending. For each l_m-constrained simulation (*i.e.*, denoted by $\{m\}$), the biased distribution of the distance fluctuation of $\rho_{\{m\}}(d)$ was obtained. Theoretically, the regional unbiased $\mathcal{A}(d)$ can be obtained by $\mathcal{A}(d) = -\beta^{-1} \ln \rho_{\{m\}}(d) - (\kappa_{\text{u}}/2)\left(d_{\{m\}} - l_m\right)^2 + \mathcal{A}_{\{m\}}$, where $\mathcal{A}_{\{m\}}$ is an undetermined shift. The unbiased distribution of the distance fluctuation $\rho(d)$ and global $\mathcal{A}(d)$ were obtained by weighted histogram analysis method using `g_wham` [24, 25], which optimizes the shifts to minimize the statistical errors of $\sigma^2(\rho(d))$ [26]. During our analysis, the final free energy difference profile reference to its global energy minimal state was evaluated at 200 discrete points, then further smoothed by cubic spline interpolation (*i.e.*, denoted by

$\Delta\mathcal{A}(d)$), from which the force-distance curve could be obtained by $f(d) = -\Delta\mathcal{A}'(d)$.

The umbrella sampling simulations were performed for twelve l_m-constrained DNA ($m = 1, 2, \cdots, 12$) (*i.e.*, l_m in descending order as m increases), which lead to nine intact DNA ($m = 1, 2, \cdots, 9$) and three DNA containing disrupted basepairs in the region of $11^{\text{th}} - 13^{\text{th}}$ basepairs ($m = 10, 11, 12$) in the last 20 ns of total 50 ns l_m-constrained simulations. The inset of Fig. 4 shows $\Delta\mathcal{A}(d)$ of B-DNA obtained from the nine intact DNA (dark red solid line), which contains a single energy minimal (set as 0 $k_{\text{B}}T$) at $d_0 \approx 5.43$ nm. A DNA rise of ~ 0.32 nm/bp estimated from d_0 is consistent with expected DNA rise of 0.33 ± 0.02 nm/bp in the B-form DNA duplex [27]. Similarly, $\Delta\mathcal{A}(d)$ for defect-containing DNA (dark red dotted line) was obtained using the three defected DNA, which has an apparently smaller slope than $\Delta\mathcal{A}(d)$ of B-DNA. Because the umbrella sampling analysis was performed separately for the two types of DNA, the two $\Delta\mathcal{A}(d)$ profiles have an undetermined offset from each other. We shifted $\Delta\mathcal{A}(d)$ of defected DNA to match $\Delta\mathcal{A}(d)$ of B-DNA at their overlapping region. We note that the shift in $\Delta\mathcal{A}(d)$ does not affect calculation of $f(d)$.

The main of Fig. 4 shows $f(d)$ of B-DNA (dark red solid line). It overlaps the data obtained by direct readout $f(\langle d_{\{m\}} \rangle) = \langle \kappa_{\text{u}} \times (d_{\{m\}} - l_m) \rangle$ (dark red $\bullet$), indicating that the umbrella sampling analysis is statistically sufficient. As expected, at the equilibrium distance $d_0 \approx 5.43$ nm, $f(d_0) = 0$ pN. For d slightly shorter than d_0, $f(d)$ increase linearly with decreasing d. The axial Young's modulus of DNA is estimated to be $Y = (\Delta f/\Delta d)\,(L/S) \approx 300$ pN/nm^2 from this linear stress-strain relation, where the contour length $L \approx d_0$, cross section $S = \pi R^2$ and radius $R = 1$ nm. The bending persistence length is estimated to be $A = \beta Y I \approx 57.0$ nm, which is very close to 53.4 ± 2.3 nm measured in previous single-DNA stretching experiments [28].

After initial linear force shooting up, the $f(d)$ profile becomes nonlinear with reduced slope in $4.8 > d > 4.6$ nm, which corresponds to a buckling force, f_{c}, in the range of $70 - 85$ pN. This behavior can be explained by Euler instability of ideal elastic rod, which predicts a critical force of the onset of the rod bending (*i.e.*, buckling transition), $f_{\text{c}} = \beta^{-1}\pi^2 A/L^2$ when $L \ll A$, where A is bending persistence length and L is DNA contour length. Using the simulated $A \approx 57.0$ pN, f_{c} estimated to be 79.1 pN, which is in agreement with the simulation results. The success in predicting the Young's modulus and the buckling transition force of B-form DNA indicates that the force field is suitable for simulating large scale of DNA mechanical properties and the overall shape of DNA has reached equilibrium over a wide

range of bending constraint within our simulation time.

Similar l_m-constrained simulations were also performed for defected DNA. $f(d)$ obtained by $-\Delta\mathcal{A}'(d)$ (dark red dotted line) and by direct readout (corresponding dark red $\bullet$) also agree with each other. The results reveal a significantly decreased $f(d)$ by ~ 50 pN compared to B-DNA force plateau after buckling transition, indicating that the defected DNA is more flexible than B-DNA. Comparing against B-DNA, $f(d)$ obtained for the defected DNA has a more rugged profile. This is because the defected DNA do not have well defined structures, with different defected forms and varying level of transient stacking with nearby basepairs.

D. Effects of nick on the micromechanics of sharply bent DNA

In order to obtain insights into the experimental observed mechanical anomaly of sharply bent DNA that contained nicks, we investigated the effects of nick on the micromechanics of sharply bent DNA. We first performed MD simulations with zero-length spring constraint (under $\kappa = 28.2$ pN/nm) to yield sharply bent conformations for four DNA containing a single nick at different locations along the top strand (see Supplemental Fig. 3 [22]), which are between the 6^{th} and 7^{th}, 8^{th} and 9^{th}, 11^{th} and 12^{th}, and 13^{th} and 14^{th} basepairs, explicitly. During simulation, the inter-base distance between the adjacent C4' atoms along the backbone of the nicked strand, $\delta_{i,i+1}$, was monitored. Here i indexes the position of the C4' atoms counted from the $5'$ end of the nicked strand.

For all the four nicked DNA, sharp bending led to significantly increased $\delta_{i,i+1}$ that straddle the nick, indicating separation of the two nick-straddling C4' atoms and their associated bases (Fig. 5). The separation of the two C4' atoms is caused by either strand separation involving a few melted basepairs near the nick (hereafter referred to as "peeled") or by unstacked basepairs straddling the nick without hydrogen bond disruptions (hereafter referred to as "unstacked"). The selection between the two types of defects depends on the sequence of the two nick-straddling basepairs, with `GC` basepairs prone to unstack whereas `AT` basepairs prone to peel (see Supplemental Fig. 4 and 5 [22]).

Further analysis shows that the separation of the two nick-straddling C4' atoms is accompanied with a large bending angle developed at the nicked position that relaxed the rest of DNA into a less bent B-form conformation. This is demonstrated in Fig. 6(a) using the nick located between the 8^{th} and 9^{th} basepairs as an example. In the sharply bent conformation,

the 8^{th} and 9^{th} basepairs are unstacked, causing the increase in $\delta_{8,9}$. The bending angle between the 7^{th} and 10^{th} basepairs, $\theta_{7,10}$, rapidly increased from the initial value of $\sim 30^\circ$ to $\sim 150^\circ$ in 2 ns after simulation began, synchronized with the increase in $\delta_{8,9}$. It is also synchronized with relaxations of the three-basepair-step bending angles in the rest of DNA to more straight conformations, as shown by the evolutions of $\theta_{4,7}$ and $\theta_{10,13}$. For another example, similar nick promoted localized sharp bend was also observed for the case of peeling around the nick [Fig. 6(b)], using the nick located between the 11^{th} and 12^{th} basepairs that caused by disruptions of hydrogen bonds in adjacent 11^{th}, 10^{th}, 9^{th}, and 8^{th} basepairs. The development of a large bending angle around the nicked position is synchronized with the relaxation of the rest of DNA to a less bent B-form conformation as well.

Using l_m-constrained simulations with umbrella sampling analysis, similar to those used for the B-form DNA, we obtained the free energy-distance ($\Delta\mathcal{A}(d)$) and force-distance ($f(d)$) profiles for DNA containing a nick between the 11^{th} and 12^{th} basepairs (Fig. 4). Both profiles overlap with that obtained for intact nick-free DNA at weak bending, suggesting that the nicked DNA has identical bending elasticity to the B-form DNA under weak bending condition. However, increased bending led to deviation of the profiles from the B-form ones, due to unstacking of the 11^{th} and 12^{th} basepairs that occurred in the distance range of $4.0 - 5.2$ nm. Further bending ($d < 4.0$ nm) caused peeling of $1 - 3$ bp nearby basepairs. The unstacking and peeling occurring at $d < 5.2$ pN resulted in a force plateau of < 40 pN, which is significantly smaller than the buckling transition force of B-form DNA (~ 80 pN). After flexible defect was excited at the nicked site the $f(d)$ becomes rugged, similar to the profile observed for nick-free DNA with defect excited inside. Overall, these results demonstrate a nick-dependent DNA softening behavior through nick-promoted excitations of flexible defects.

The nick-dependent DNA softening appears sensitive to temperature. The same simulation for the nicked DNA at a lowered temperature of 290 K (10 K less than previous simulations) revealed that the basepairs straddling the nick remained stacked in the range of end-to-end distance tested (> 4.2 nm) even at a longer simulation time of 100 ns. This is in sharp contrast to the simulation at 300 K where flexible defects are excited at $d < 5.2$ nm within 50 ns. The resulting force-distance curve nearly overlaps with that obtained for the B-form DNA including the region after the buckling transition. The slightly lower $f(d)$ profile at 290 K than that at 300 K is due to the temperature dependency of the

buckling transition force given by $f_c = \beta^{-1}\pi^2 A/L^2$. This result indicates that the lowered temperature strongly suppresses the nick-dependent excitations of flexible defects.

III. DISCUSSION

In order to obtain new insights into the debating problem regarding the anomalous DNA bend elasticity observed in recently reported sharp DNA bending experiments, we performed extensive MD simulations and umbrella sampling studies on contractile springs induced DNA bending at a temperature of 300 K. We observed excitation of flexible DNA defects with disruptions of a few basepairs when the DNA was bent sharply enough. Further, when the DNA contained a nick, flexible defects were excited at the nicked location requiring much less DNA bending level compared to DNA without nicks. For 20 bp nicked DNA, defects were excited at a force $\sim$ 40 pN, which is much less than the B-DNA buckling transition force at $\sim$ 80 pN. Importantly, this nick-dependent defect excitation is very sensitive to temperature – reducing temperature by 10 degrees to 290 K greatly suppresses the nick-dependent excitations of flexible defects. These results have important implications to the understanding of recent experiments and theoretical discussions, as detailed below.

The debating problem began with a "j-factor" measurement that reported an anomalously high DNA looping probability of $94-116$ bp [8] (see Appendix D for further details). In such experiments, a DNA fragment with short complementary ssDNA overhangs at the two ends was used. In a solution of such DNA molecules at a concentration $c = N/V$ (N is the number of molecule and V is the volume), a terminus of a molecule can hybridize with a complementary terminus from the same molecule (*i.e.*, looping) or from another molecule (*i.e.*, dimerization), driven by thermal fluctuation. Theoretically, if hybridization between complementary DNA ends can occur without any conformational constraint, then $K_{\rm loop}/K_{\rm dimer} = \rho^{\rm E}\left(\boldsymbol{R}=\mathbf{0}\right)/c$, where $\boldsymbol{R}$ is the distance vector between the two ends, which results in experimental determination of looping probability density as: $\rho^{\rm E}\left(\mathbf{0}\right) = K_{\rm loop}/K^0_{\rm dimer}$. Here $K^0_{\rm dimer} = K_{\rm dimer}/c$ denotes the dimerization rate per unit concentration of DNA. The ratio $j = K_{\rm loop}/K^0_{\rm dimer}$ is often referred to the "j-factor", which has a dimension of concentration [4, 8, 29]. Often, molar concentration is used in experiments, which leads to an additional factor of Avogadro's number.

However, hybridization between two complementary DNA ends actually imposes certain

orientational constraints on the two meeting DNA ends. Assuming that the hybridizing DNA ends for both looped and dimerized DNA are in parallel to each other and twisted to match the B-form conformation (hereafter we call this constraint as twist-matching parallel boundary condition, denoted by Ω), the measured looping probability density is related to the j-factor by: $\rho^{\mathrm{E}}(\mathbf{0}) = j/(8\pi^2)$, where the factor $(4\pi \times 2\pi)^{-1}$ comes from the Ω constraint on the dimeric molecules.

The assumption of the Ω boundary constraints for both hybridized dimeric and looped DNA has been implied (although might not be explicitly mentioned) in interpreting the results obtained from all previous j-factor experiments of DNA. Therefore, the DNA looping probability density theoretically calculated by the WLC model that takes into consideration of the twist energy of DNA should be related to j by equation:

$$\rho_{\Omega}(\mathbf{0}) = \rho^{\mathrm{E}}(\mathbf{0}) = \frac{j}{8\pi^2}. \tag{1}$$

Based on such j-factor measurements and theoretical interpretation, the DNA persistence length was determined in the range of $45 - 55$ nm, over a wide contour length range (> 200 bp) in normal solution conditions [12, 13]. The agreement between the measured values of A and that from single-DNA stretching experiments validates the Ω boundary condition for DNA larger than 200 bp.

However, for shorter DNA fragments around 100 bp, the j-factor measurements reported a DNA looping probability density that are several orders of magnitude larger than that predicted by WLC model with $A \approx 50$ nm [8]. This disagreement between experiments and the WLC model prediction has led to a decade of confusion on its nature. There are two alternative possibilities that may cause such anomaly: (i) It is an intrinsic elastic response of dsDNA under sharp bending condition, which might be caused by bending induced flexible defect excited inside the DNA as proposed by several groups [8, 17–19]; (ii) The Ω boundary condition assumption is no longer valid for the hybridized looped DNA when DNA is sharply bent. In the latter case, equation 1 used to extract the mechanical properties of DNA is no longer valid. In previous studies, researchers have focused their discussions on the possibility (i), while the possibility (ii) has not been considered as a possible cause of the observed anomalously high looping probability density prior to this work.

In this work, using MD simulation we demonstrated that a pre-existing nick may facilitate excitation of flexible defects at the nicked location when the DNA is sharply bent, by either

unstacking the two adjacent basepairs straddling the nick, or further strand peeling near the nick. This result suggests that the two pre-existing nicks in the hybridized loop may cause DNA kink in sharply bent DNA minicircles; thereby violating the Ω boundary condition. As a result, to compare with the j-factor measurement, the looping probability density should be calculated based on a different boundary condition ξ. As shown in previous theoretical predictions [18, 30, 31], if the two ends of the same DNA can meet in a kinked conformation, the looping probability density is greatly increased compared to that under the Ω boundary condition (*i.e.*, $\rho_{\xi}(\mathbf{0}) > \rho_{\Omega}(\mathbf{0})$). In the extreme case when the two ends can meet with arbitrary angle, the looping probability density can be at least three orders of magnitude larger than that under the Ω boundary condition for < 100 bp DNA fragments. Further, as soon as kinks are excited at the nicked site, the rest of DNA is relaxed, so that excitation of defect inside the nick-free dsDNA region is suppressed.

This mechanism naturally explained the j-factor measurement results for ~ 100 bp short DNA fragments reported by Cloutier *et al.* using ligation approach with 4 nt overhangs [8, 32]. j-factor measurement reporting softening anomaly of short DNA was also done based on single-molecule Frster resonance energy transfer (smFRET) assay without a need to use ligase to close the hybridized loops [9, 33]. However, that assay used long overhangs (~ 10 nt) to stabilize the loop, resulting in potential partially-hybridized looped intermediates that may contribute to the observed FRET efficiency that was used to calculate the j-factor. Therefore, direct comparison between the apparent j-factor obtained from that assay with theoretical prediction is non-trivial.

A disagreeing result was reported in a j-factor measurement for $94-116$ bp DNA using 4 nt overhangs by Du *et al.*, which found that the DNA looping probability density follows the canonical WLC polymer model [29]. However, that experiment was performed at 21°C, nine degrees below that used in the experiments by Coutier *et al.* Therefore, this disagreement may actually reflect a temperature sensitivity in such experiments. Indeed, our simulation revealed that decreasing temperature from 300 K to 290 K, the nick-dependent defect excitation in sharply bent DNA is greatly suppressed over a wide bending constraint. Therefore, the Ω boundary condition for hybridized looped DNA becomes more likely at lowered temperatures, which provides an plausible explanation to the conflicting j-factor measurement results.

Elastic anomaly of DNA was also revealed by analyzing the unlooping rate of a hybridized

looped DNA or looping rate of an originally unlooped DNA using smFRET approach. Both assays suggested that there exist a critical contour length of DNA (< 100 bp), below which the dependency of unlooping (or looping) rate on DNA size indicates a softer DNA backbone than that predicted by the WLC model with 50 nm persistence length [9, 33]. Again, the pre-existing nicks of the hybridized DNA loop may develop kinks at the nicked location, resulting in the observed anomaly. In addition to DNA cyclization experiments, Hao *et al.* also reported softening elastic anomaly when they bent a short DNA fragment using a short ssDNA connected the two dsDNA ends [15, 16]. By experimental design their DNA construct contained a pre-existing nick in the middle; therefore, their result can also be explained by the nick-dependent kinkable/flexible defect excitation rather than reflecting an intrinsic elastic response of DNA duplex under severe bending.

The micromechanics of DNA bending was also studied by analyzing the bending angle distribution over short DNA contour length from DNA conformations imaged with Atomic force microscopy (AFM) imaging in-air. In such assay, the DNA molecules were adsorbed on mica surface using $MgCl_2$ under an assumption that the conformations have been relaxed in 2-dimension. That experiment reported that $5 - 10$ nm DNA fragments have a significantly higher probability for larger bending angle than that predicted by the canonical WLC polymer model [34]. However, such experiment cannot exclude the possibility that perturbation during sample drying processes might cause rare large DNA kinks. In fact, it has been demonstrated in a more recent AFM imaging experiment carried out in solution that reported a normal bending angle distribution expected from the canonical WLC polymer model for ~ 10 nm DNA fragments [35].

In DNA without nicks, our simulations suggest that flexible defect excitation can still be excited for more severely bent DNA, which is consistent with two recent experiments. Du *et al.* reported that covalently ligated $63-65$ bp DNA minicircles could be digested by the BAL-31 nuclease [20, 21], indicating ssDNA in these DNA minicircles. In another experiment, Shroff *et al.* bent a nick-free 25 bp dsDNA fragment using a 12 nt ssDNA connected the two dsDNA ends [14]. Assuming dsDNA is intact, its internal tension is expected to be around bucking transition force ~ 30 pN. This corresponds to ssDNA separation of ~ 6 nm based on phenomenological ssDNA force extension model [36], similar to that between two points separated by 25 bp in a 64 bp DNA minicircle in a planar circle conformation (*i.e.*, $L \sin(25\pi/64)/\pi \approx 6$ nm, where L is the contour length of the 64 bp minicircle).

But the measured tension in the ssDNA was shown to be 6 ± 5 pN, a few times smaller than aforementioned critical bending force, while the distance between the two dsDNA ends was estimated to be less than 4 nm, which revealed DNA anomalous elastic responses. Together, these results indicate that basepair disruption can occur in the level of DNA bending comparable to that in $63 - 65$ bp minicircles [20]. However, whether such defect can be excited in nick-free ~ 100 bp minicircles and how the excitation depends on solution condition remain unsolved.

It has been theoretically demonstrated that excitation of flexible mechanical defects under bending constraint could explain the anomalously high cyclization rate of ~ 94 bp DNA [17–19]. Such models typically contain two free parameters, the energy cost to excite a defect and the DNA bending flexibility of the defect. In previous discussions, these parameters were attributed to potential defect excitation inside a B-DNA. According the results from this study, most likely they should correspond to the excitation of flexible defects at the nick which takes less excitation energy compared to excitation inside a B-DNA.

In summary, our full-atom MD simulation results reveal that pre-existing nicks in a sharply bent DNA are hotspots to adsorb the bending through developing localized kinks which relaxes the rest of nick-free DNA regions in a temperature dependent manner. This finding provides a natural explanation to the DNA elastic anomaly reported in nearly all previous DNA bending experiments, where the DNA necessarily contained nicks by experimental design. As such, our results challenge the previous interpretations that suggested the observed softening anomaly is an intrinsic elastic response of dsDNA, and highlight that the micromechanics of sharply bent DNA at the level of DNA minicircles of ~ 100 bp still remains as an open question.

ACKNOWLEDGEMENTS

The authors are grateful to John Marko (Northwestern University) for valuable discussions. Support for the work was provided by National Research Foundation of Singapore through the Mechanobiology Institute at National University of Singapore (to J.Y.) and National Research Foundation Singapore through the Singapore-MIT Alliance for Research and Technology.

P.C. and L.D. contributed equally to this work.

Appendix A: DNA constructs and molecular dynamics simulations

The 20 bp DNA sequence, equation A1, used in the spring-constrained simulations is extracted from the 94 bp E6-94 DNA sequence used in the DNA cyclization experiment [8],

$$\begin{matrix} 5' - \texttt{GTGCGCACGAAATGCTATGC} - 3' \\ 3' - \texttt{CACGCGTGCTTTACGATACG} - 5' \end{matrix} . \tag{A1}$$

The basepairs are indexed by i, counted from $5'$ to $3'$ end of the top strand of the dsDNA segments. Contractile springs with various equilibrium length or various spring constants are connected to the bases of 2^{nd} and 19^{th} basepairs to induce bending, and force is distributed among their base atoms according to atomic weights. A smoothly bent B-form DNA was generated by the program `X3DNA` [37] as the initial conformation for the simulation.

The MD simulations were prepared and ran using the latest `GROMACS` version 4.5.5 [38–40] under the newest Parm99 force field with ParmBSC0 corrections [41, 42]. Before starting any simulation, a basic simulating unit (*i.e.*, unit cell) was properly constructed. Firstly, an initial atomic DNA structure with targeted sequence and shape was generated using `X3DNA` [43]. Secondly, this initial structure was centered within a minimal unit cell. Our simulations usually utilized rhombic dodecahedron (*i.e.*, $\sim 71\%$ of cubic unit cell volume), whose inscribed sphere diameter equals to the largest DNA extension plus an additional 3.2 nm for buffering purpose. Next, this unit cell was further prepared by filling the empty space with TIP3P water [44], neutralizing the negative charges on DNA using sodium counter-ions, and replacing some water molecules by sodium chloride to achieve 150 mM ionic strength. Lastly, it was finalized by energy minimization using the steepest descent method to remove any energy unfavorable close contacts.

Based on such prepared unit cell, molecular trajectories were self evolved according to Newton's law of motion, given a set of randomized velocities sampled from Maxwell-Boltzmann distribution, and designed constraints, such as contractile springs. Before collecting conformational evolutions, the unit cell was brought to correct ensemble, through thermolization using 200 ps velocity rescaling and 200 ps Parrinello-Rahman pressure coupling simulations to adjust its temperature and volume [45, 46]. After these, usually a 70 ns MD simulation, which includes 50 ns equilibration stage and 20 ns production stage, was executed using periodic boundary conditions, under NVT ensemble, with constant temperature of 300 K (or 290 K) and volume up to ~ 1170 nm^3. And, the conformational

representatives during the production stage were used for extracting interested ensemble averages, for instance, the averaged end-to-end distances, $\langle d \rangle$. Prior to any constrained simulations, an unconstrained 20 bp DNA simulation has been conducted for 70 ns as control, during which DNA maintained a regular helical structure with expected helical repeat and pitch (see Supplemental Fig. 6 [22]).

Appendix B: Basepair coordinates

Assigning a basepair coordinate to the group of thermally fluctuated atoms is the key to bridge from MD raw trajectories to DNA macroscopic behaviors, such as bending dynamics.

An ideal Watson-Crick basepair [47] was fitted to each observed instant atomic arrangements during MD simulations by minimizing the sum of squares of their residual errors. This least-square fitting was implemented by Horn in 1987 [48] through finding a closed-form solution of the ideal basepair absolute orientation against such instant atomic arrangements. A sketch of this ideal basepair coordinates is shown (Fig. 7). For this `GC` Watson-Crick basepair, a right-handed coordinate frame as described by Olson *et al.* [27] was attached to it, with $\hat{x}_i$ pointing to the major groove, $\hat{y}_i$ pointing to the backbone of the top strand, and $\hat{z}_i = \hat{x}_i \times \hat{y}_i$ describing the normal direction of the Watson-Crick basepair, where i denotes the i^{th} basepair. This process is achieved using `X3DNA` software [37, 43].

After this, some macroscopic configuration information can be extracted using local coordinates. For example, the bending angle between i^{th} and $(i+\Delta)^{\text{th}}$ basepairs, defined by $\theta_{i,i+\Delta} = \cos^{-1}(\hat{z}_i \cdot \hat{z}_{i+\Delta})$, where $i = 2, 3, \cdots, 19 - \Delta$, can be calculated for any instant conformation of DNA.

Appendix C: Location of defects

Figure 8(a) plots the hydrogen bonding profiles, $\langle \min(h_{i,j}) \rangle$ and $\langle \max(h_{i,j}) \rangle$ *v.s.* i averaged over the last 20 ns, for all twelve independent simulations with $\kappa > 25.0$ pN/nm. This "histogram" reveals that the disrupted basepairs appeared around the same region near DNA center that happen to be `AT`-rich (*i.e.*, $5' - \texttt{AAAT} - 3'$, the $10^{\text{th}} - 13^{\text{th}}$ basepairs).

One possible cause to the central localization of basepair disruptions is the largest curvature at the center under bending constraints. Assuming the two ends of the homogeneous

WLC polymer meets before any defects appears, we can orient its elastic energy minimal rigid path on xy-plane by setting its terminal cross point as origin, center point on the positive side of y-axis, then this rigid path breaks into two reflection symmetric halves, as shown in Fig. 9. By defining the angle between unit tangent vector $\hat{t}(s)$ (along the half path in Quadrant I) and x-axis as $\upsilon(s)$, we have its relationship with curvature [49] as,

$$L^2 \left(\frac{\partial \hat{t}(s)}{\partial s} \right)^2 = -\lambda \cos\left(\upsilon(s)\right) + c \tag{C1}$$

, where L is the contour length, $\lambda > 0$ is a Lagrange multiplier, and $c > 0$ is integration constant. Following above equation, the curvature is maximized at the center, as $\upsilon\left(L/2\right) = \pi$ by symmetry.

Alternatively, it may be due to the less stable `AT` non-covalent interactions in the middle of our DNA. Based on the unified NN basepair parameters by SantaLucia *et al.* [50], melting `AT` next to `AT` basepair (*i.e.*, $\Delta G < 2\ k_{\mathrm{B}}T$) is generally easier than melting `AT` next to `GC` or melting `GC` next to `AT` basepairs (*i.e.*, $3 > \Delta G > 2\ k_{\mathrm{B}}T$), while melting `GC` next `GC` basepairs is hardest (*i.e.*, $\Delta G > 3\ k_{\mathrm{B}}T$).

To see which factor predominates, we shifted the entire sequence tail-to-head by 2 bp and replaced the central `AT`-rich island at $10^{\mathrm{th}} - 13^{\mathrm{th}}$ basepairs with $5' - \mathtt{CGAA} - 3'$. Five independent destructive MD simulations under different bending constraints with $\kappa > 25$ pN/nm were conducted for 70 ns each. The overlay of their resulting hydrogen bonding profiles [Fig. 8(b)] shows that the basepair disruptions still occur at the central region, mainly at the $10^{\mathrm{th}} - 11^{\mathrm{th}}$ basepair (*i.e.*, `GC` base-pairing), and 12^{th} basepair (*i.e.*, `AT` base-pairing). Taken together, these results suggest that the central localization of the basepair disruptions is mainly caused by the high curvature at the center, while the sequence effects are minor under our bending constructs.

Appendix D: DNA j-factor experiments

Considering a DNA molecule with two ends denoted by "A" and "B", respectively. The DNA looping probability density, $\rho\left(\mathbf{0}\right)$, is the probability density when the two ends of the same DNA molecule meet. In other words, $P_{\mathrm{loop}} = \rho\left(\mathbf{0}\right)\delta V$ is the probability to find the end "B" in an infinitesimal volume δV in the vicinity of the end "A" of the same DNA . In the presence of the N identical DNA molecules in a total volume of V, the probability of

finding an end "B" from another molecule in the same vicinity around the end "A" of the target DNA is $(N/V)\,\delta V = c \cdot \delta V$. In order to determine $\rho\,(\mathbf{0})$, a cyclization approach has been proposed to chemically trap (such as ligation) the "A-B" ends in δV, which results in either looped DNA or dimerized DNA molecules with reaction rates of $K_{\rm loop}$ and $K_{\rm dimer} = c \cdot K^0_{\rm dimer}$, respective, where $K^0_{\rm dimer}$ denotes the dimerization rate per unit concentration of DNA. Theoretically, $K_{\rm loop}/K_{\rm dimer} = \rho\,(\mathbf{0})/c$, which results in experimental determination of looping probability density as: $\rho^{\rm E}\,(\mathbf{0}) = K_{\rm loop}/K^0_{\rm dimer}$. The ratio $K_{\rm loop}/K^0_{\rm dimer}$ is often referred to as the "j-factor" [4, 8, 29].

A typical j-factor measurement approach is based on using ligase to covalently link the DNA ends. This method requires two short complementary ssDNA overhangs at the two DNA ends, which transiently hybridize the "A-B" ends into a conformation suitable for a subsequent ligation reaction. A prerequisite for such measurement is that the hybridized loop or hybridized dimer must be weak interactions, allowing reversible unlooping or undimerzation to achieve pre-equilibration before the ligation reaction [4, 12]. What measured in such experiments are rates of covalent closure of hybridized loop $K'_{\rm loop}$ and hybridized dimer $K'_{\rm dimer}$. With an additional assumption that $K'_{\rm loop}/K'_{\rm dimer} = K_{\rm loop}/K_{\rm dimer}$, the looping probability density $\rho^{\rm E}\,(\mathbf{0})$ can be determined.

Further, hybridization also imposes a constraint on the orientations of the hybridized "A-B" ends. In the case of dimerization, which does not involve any DNA bending or twisting, the hybridized DNA assumes a straight B-form conformation, as suggested in our simulation. This results in two requirements on termini orientations: (i) the hybridized ends "A" and "B" should be parallel to each other; (ii) the ends must be helically phase matching which constraints the axial twist degree of freedom of one molecule to the other (Fig. 10). Together, these requirements imply the probability density of the hybridizable end "B" from another molecule is $c/\,(4\pi \times 2\pi)$. As a result, $\rho^{\rm E}\,(\mathbf{0}) = (8\pi^2)^{-1}\,K_{\rm loop}/K^0_{\rm dimer}$. In the main text, we have referred such boundary constraint as the "Ω" boundary condition.

Hybridization may also impose a constraint on the orientations of the hybridized "A-B" ends in the hybridized looped DNA. In the case of large loop ($L > A_{\rm Tw}$, where $A_{\rm Tw} \sim 100$ nm is the twist persistence length), the same Ω boundary condition should apply due to the decreased twist energy in large DNA loops. In order to extract the DNA micromechanical properties, such as persistence lengths, one should calculate the looping probability density based on the WLC model $\rho^{\rm WLC}\,(\mathbf{0})$ under the Ω boundary condition treating the DNA

bending and twisting persistence lengths as free parameters, and compare it with the experimentally measured value $\rho^{\mathrm{E}}(\mathbf{0})$. However, for small DNA loops, the Ω boundary condition may not hold, due to the increased bending energy in the loops which may cause defect excitation at the nicks (as suggested in our simulations). In this case, $\rho^{\mathrm{WLC}}(\mathbf{0})$ should be calculated under a different boundary condition $\xi \neq \Omega$, which has been ignored in previous discussions.

---

[1] Timothy J Richmond and Curt A Davey. The structure of DNA in the nucleosome core. *Nature*, 423(6936):145–150, May 2003.

[2] S Oehler, M Amouyal, P Kolkhof, B von Wilcken-Bergmann, and B Muller-Hill. Quality and position of the three lac operators of E. coli define efficiency of repression. *EMBO J.*, 13(14): 3348–3355, July 1994.

[3] Paul J Hagerman. Flexibility of DNA. *Annu. Rev. Biophys. Biophys. Chem.*, 17(1):265–286, 1988.

[4] D Shore, J Langowski, and R L Baldwin. DNA flexibility studied by covalent closure of short fragments into circles. *Proc. Natl. Acad. Sci. U. S. A.*, 78(8):4833–4837, January 1981.

[5] M Doi and S F Edwards. *The theory of polymer dynamics*. Clarendon: Oxford, 1986.

[6] S B Smith, L Finzi, and C Bustamante. Direct mechanical measurements of the elasticity of single DNA molecules by using magnetic beads. *Science*, 258(5085):1122–1126, January 1992.

[7] John F Marko and Eric D Siggia. Stretching DNA. *Macromolecules (Washington, DC, U. S.)*, 28(26):8759–8770, 1995.

[8] Timothy E Cloutier and Jonathan Widom. Spontaneous Sharp Bending of Double-Stranded DNA. *Mol. Cell*, 14(3):355–362, May 2004.

[9] Reza Vafabakhsh and Taekjip Ha. Extreme Bendability of DNA Less than 100 Base Pairs Long Revealed by Single-Molecule Cyclization. *Science*, 337(6098):1097–1101, January 2012.

[10] Karolin Luger, Armin W Mäder, Robin K Richmond, David F Sargent, and Timothy J Richmond. Crystal structure of the nucleosome core particle at 2.8[thinsp]A resolution. *Nature*, 389(6648):251–260, September 1997.

[11] Curt A Davey, David F Sargent, Karolin Luger, Armin W Maeder, and Timothy J Richmond. Solvent Mediated Interactions in the Structure of the Nucleosome Core Particle at

1.9Å Resolution. *J. Mol. Biol.*, 319(5):1097–1113, June 2002.

[12] David Shore and Robert L Baldwin. Energetics of DNA twisting: I. Relation between twist and cyclization probability. *J. Mol. Biol.*, 170(4):957–981, November 1983.

[13] William H Taylor and Paul J Hagerman. Application of the method of phage T4 DNA ligase-catalyzed ring-closure to the study of DNA structure: II. NaCl-dependence of DNA flexibility and helical repeat. *J. Mol. Biol.*, 212(2):363–376, March 1990.

[14] Hari Shroff, Björn M Reinhard, Merek Siu, Harish Agarwal, Andrew Spakowitz, and Jan Liphardt. Biocompatible Force Sensor with Optical Readout and Dimensions of 6 nm3. *Nano Lett.*, 5(7):1509–1514, August 2005.

[15] Hao Qu, Chiao-Yu Tseng, Yong Wang, Alex J Levine, and Giovanni Zocchi. The elastic energy of sharply bent nicked DNA. *EPL*, 90(1):18003, April 2010.

[16] Hao Qu, Yong Wang, Chiao-Yu Tseng, and Giovanni Zocchi. Critical Torque for Kink Formation in Double-Stranded DNA. *Phys. Rev. X*, 1(2):021008, 2011.

[17] Jie Yan and John F Marko. Localized Single-Stranded Bubble Mechanism for Cyclization of Short Double Helix DNA. *Phys. Rev. Lett.*, 93(10):108108, January 2004.

[18] Jie Yan, Ryo Kawamura, and John F Marko. Statistics of loop formation along double helix DNAs. *Phys. Rev. E*, 71(6):061905, January 2005.

[19] Paul A Wiggins, Rob Phillips, and Philip C Nelson. Exact theory of kinkable elastic polymers. *Phys. Rev. E*, 71(2):021909, January 2005.

[20] Q Du, A Kotlyar, and A Vologodskii. Kinking the double helix by bending deformation. *Nucleic Acids Res.*, 36(4):1120–1128, December 2007.

[21] Alexander Vologodskii and Maxim D Frank-Kamenetskii. Strong bending of the DNA double helix. *Nucleic Acids Res.*, 41(14):6785–6792, August 2013.

[22] See Supplemental Material at URL for Supplemental Figs. 1-6 on B-DNA initial structure, end-to-end distances under varies κ, nicked DNA initial structure, defected nicked DNA hydrogen profiles, illustrations on types of defected nicked DNA and B-DNA regular helical shape.

[23] Célia Fonseca Guerra, F Matthias Bickelhaupt, Jaap G Snijders, and Evert Jan Baerends. The Nature of the Hydrogen Bond in DNA Base Pairs: The Role of Charge Transfer and Resonance Assistance. *Chem.–Eur. J.*, 5(12):3581–3594, January 1999.

[24] Shankar Kumar, John M Rosenberg, Djamal Bouzida, Robert H Swendsen, and Peter A Koll-

man. THE weighted histogram analysis method for free-energy calculations on biomolecules. I. The method. *J. Comput. Chem.*, 13(8):1011–1021, January 1992.

[25] Jochen S Hub, Bert L de Groot, and David van der Spoel. g_wham—A Free Weighted Histogram Analysis Implementation Including Robust Error and Autocorrelation Estimates. *J. Chem. Theory Comput.*, 6(12):3713–3720, January 2010.

[26] G M Torrie and J P Valleau. Nonphysical sampling distributions in Monte Carlo free-energy esUmbrella sampling. *J. Comput. Phys.*, 23(2):187–199, February 1977.

[27] Wilma K Olson, Manju Bansal, Stephen K Burley, Richard E Dickerson, Mark Gerstein, Stephen C Harvey, Udo Heinemann, Xiang-Jun Lu, Stephen Neidle, Zippora Shakked, Heinz Sklenar, Masashi Suzuki, Chang-Shung Tung, Eric Westhof, Cynthia Wolberger, and Helen M Berman. A standard reference frame for the description of nucleic acid base-pair geometry. *J. Mol. Biol.*, 313(1):229–237, October 2001.

[28] C Bustamante, J F Marko, E D Siggia, and S Smith. Entropic Elasticity of λ-Phage DNA. *Science*, 265(5178):1599–1600, January 1994.

[29] Quan Du, Chaim Smith, Nahum Shiffeldrim, Maria Vologodskaia, and Alexander Vologodskii. Cyclization of short DNA fragments and bending fluctuations of the double helix. *Proc. Natl. Acad. Sci. U. S. A.*, 102(15):5397–5402, January 2005.

[30] Jiro Shimada and Hiromi Yamakawa. Ring-closure probabilities for twisted wormlike chains. Application to DNA. *Macromolecules (Washington, DC, U. S.)*, 17(4):689–698, July 1984.

[31] Hu Chen and Jie Yan. Effects of kink and flexible hinge defects on mechanical responses of short double-stranded DNA molecules. *Physical Review E*, 77(4):041907, April 2008.

[32] Timothy E Cloutier and Jonathan Widom. DNA twisting flexibility and the formation of sharply looped protein-DNA complexes. *Proceedings of the National Academy of Sciences*, 102(10):3645–3650, March 2005.

[33] Tung T Le and Harold D Kim. Probing the elastic limit of DNA bending. *Nucleic Acids Res.*, 42(16):10786–10794, December 2014.

[34] Paul A Wiggins, Thijn van der Heijden, Fernando Moreno-Herrero, Andrew Spakowitz, Rob Phillips, Jonathan Widom, Cees Dekker, and Philip C Nelson. High flexibility of DNA on short length scales probed by atomic force microscopy. *Nat. Nanotechnol.*, 1(2):137–141, November 2006.

[35] Alexey K. Mazur and Mounir Maaloum. Dna flexibility on short length scales

probed by atomic force microscopy. *Phys. Rev. Lett.*, 112:068104, Feb 2014. doi: 10.1103/PhysRevLett.112.068104.

[36] Simona Cocco, Jie Yan, Jean-Francois Léger, Didier Chatenay, and John Marko. Overstretching and force-driven strand separation of double-helix DNA. *Physical Review E*, 70(1):011910, July 2004.

[37] Xiang-Jun Lu and Wilma K Olson. 3DNA: a software package for the analysis, rebuilding and visualization of threedimensional nucleic acid structures. *Nucleic Acids Res.*, 31(17): 5108–5121, January 2003.

[38] Berk Hess, Carsten Kutzner, David van der Spoel, and Erik Lindahl. GROMACS 4: Algorithms for Highly Efficient, Load-Balanced, and Scalable Molecular Simulation. *J. Chem. Theory Comput.*, 4(3):435–447, March 2008.

[39] David van der Spoel, Erik Lindahl, Berk Hess, Gerrit Groenhof, Alan E Mark, and Herman J C Berendsen. GROMACS: Fast, flexible, and free. *J. Comput. Chem.*, 26(16):1701–1718, January 2005.

[40] Sander Pronk, Szilárd Páll, Roland Schulz, Per Larsson, Pär Bjelkmar, Rossen Apostolov, Michael R Shirts, Jeremy C Smith, Peter M Kasson, David van der Spoel, Berk Hess, and Erik Lindahl. GROMACS 4.5: a high-throughput and highly parallel open source molecular simulation toolkit. *Bioinformatics*, 29(7):845–854, January 2013.

[41] Thomas E Cheatham III, Piotr Cieplak, and Peter A Kollman. A Modified Version of the Cornell et al.Force Field with Improved Sugar Pucker Phases and Helical Repeat. *J. Biomol. Struct. Dyn.*, 16(4):845–862, February 1999.

[42] Alberto Pérez, Iván Marchán, Daniel Svozil, Jiri Sponer, Thomas E Cheatham, III, Charles A Laughton, and Modesto Orozco. Refinement of the AMBER Force Field for Nucleic Acids: Improving the Description of α/γ Conformers. *Biophys. J.*, 92(11):3817–3829, June 2007.

[43] Xiang-Jun Lu and Wilma K Olson. 3DNA: a versatile, integrated software system for the analysis, rebuilding and visualization of three-dimensional nucleic-acid structures. *Nat. Protoc.*, 3 (7):1213–1227, July 2008.

[44] William L Jorgensen, Jayaraman Chandrasekhar, Jeffry D Madura, Roger W Impey, and Michael L Klein. Comparison of simple potential functions for simulating liquid water. *J. Chem. Phys.*, 79(2):926–935, January 1983.

[45] Giovanni Bussi, Davide Donadio, and Michele Parrinello. Canonical sampling through velocity

rescaling. *J. Chem. Phys.*, 126(1):014101, January 2007.

[46] M Parrinello. Polymorphic transitions in single crystals: A new molecular dynamics method. *J. Appl. Phys.*, 52(12):7182–7190, December 1981.

[47] Lester Clowney, Shri C Jain, A R Srinivasan, John Westbrook, Wilma K Olson, and Helen M Berman. Geometric Parameters in Nucleic Acids: Nitrogenous Bases. *J. Am. Chem. Soc.*, 118(3):509–518, January 1996.

[48] Berthold K P Horn. Closed-form solution of absolute orientation using unit quaternions. *J. Opt. Soc. Am. A*, 4(4):629–642, April 1987.

[49] Hiromi Yamakawa. Statistical Mechanics of Wormlike Chains. II. Excluded Volume Effects. *J. Chem. Phys.*, 57(7):2843–2854, October 1972.

[50] John SantaLucia. A unified view of polymer, dumbbell, and oligonucleotide DNA nearest-neighbor thermodynamics. *Proc. Natl. Acad. Sci. U. S. A.*, 95(4):1460–1465, February 1998.

FIG. 1. Overview of distinctive DNA bending behaviors under weak and strong spring constraints. Superimpositions of equilibrated DNA helical axes collected per ns in last 20 ns for each simulation. The fourteen independent MD simulations were all initiated from same initial (represented by thick red helical axis, whose atomic structure is in Supplemental Fig. 1 [22]), and their corresponding stabilized "center lines" were colored cyan for weak spring constants $\kappa = 8.3, 16.6$ pN/nm; while copper for strong bending $\kappa = 26.6, 28.2$ (five independent simulations), $29.0, 31.5, 3.2, 41.5, 49.8, 83.0$ pN/nm, respectively. When $\kappa < 20.0$ pN/nm, their center lines are uniformly bent and more straight than initial. While, when $\kappa > 25.0$ pN/nm, their center lines are non-uniformly bent and much more curved than initial.

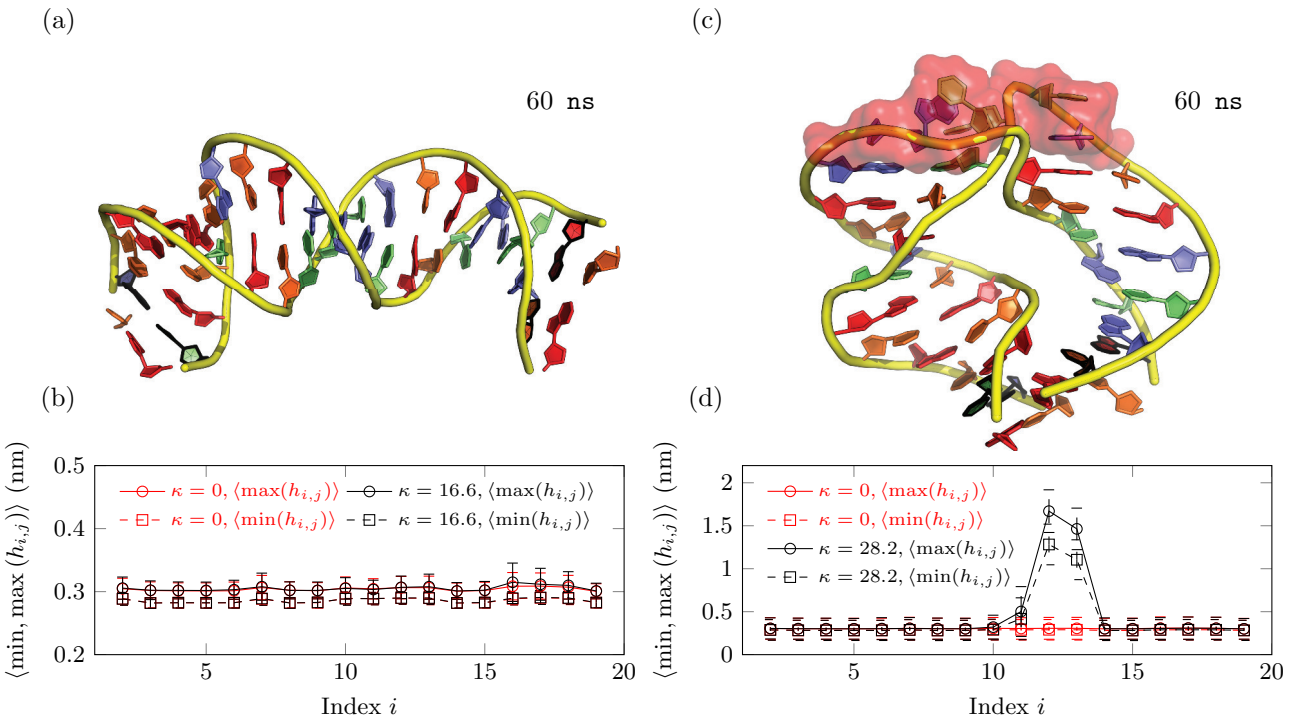

FIG. 2. Different DNA bending response under spring constraints. (a) A snapshot of a smoothly bent DNA conformation at $t = 60$ ns under a weak spring constant $\kappa = 16.6$ pN/nm. (b) Base-pairing integrity analysis, $\langle \min, \max(h_{i,j}) \rangle$ *v.s.* $i = 2, 3, \cdots, 19$ averaged over the last 20 ns. (c) A snapshot of a severely bent DNA conformation at 60 ns under a strong spring constant $\kappa = 28.2$ pN/nm, which contains a local basepair disruption in the middle. (d) $\langle \min, \max(h_{i,j}) \rangle$ averaged over the last 20 ns reveals three disrupted basepairs at $i = 11, 12, 13$, which are highlighted by red surfaces in (c).

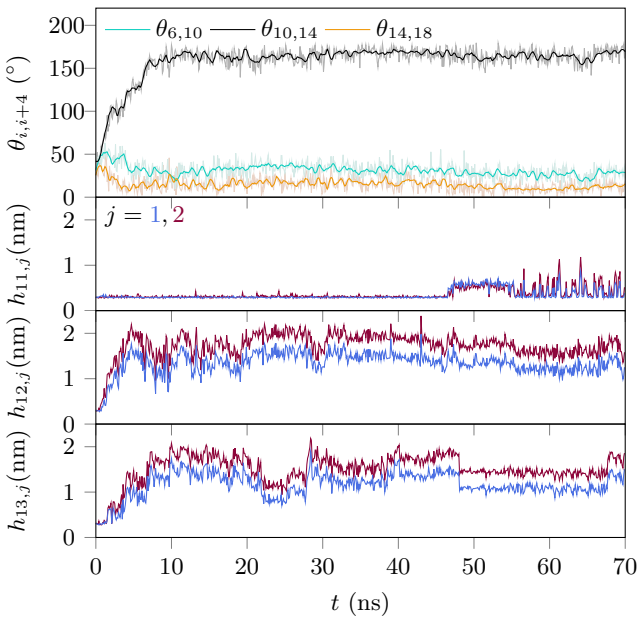

FIG. 3. 70 ns dynamics of local bending deformations and hydrogen bonding disruptions under $\kappa = 28.2$ pN/nm. Row 1: time evolution of $\theta_{10,14}$ (black) enclosing three disrupted basepairs at $i = 11, 12, 13$, which shows the kink development around defected region. The bending angle evolutions of two intact regions with same length, $\theta_{6,10}$ (cyan) and $\theta_{14,18}$ (orange), are shown for comparison. Rows $2 - 4$: time evolutions of $h_{i,j}$ for the three disrupted basepairs $i = 11, 12, 13$, which are all `AT` basepairs and involve two atom-atom distances ($j = 1$ in dark blue and $j = 2$ in dark red).

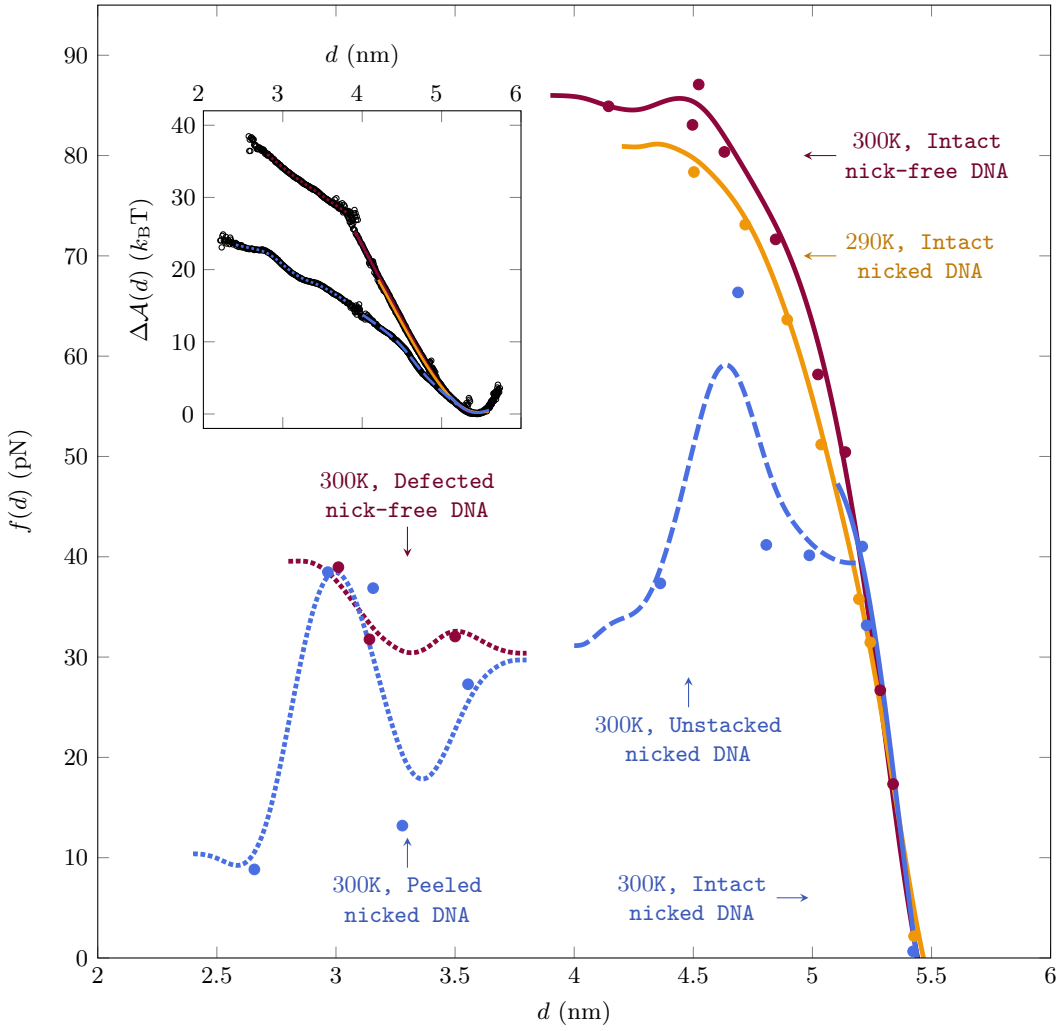

FIG. 4. $\Delta\mathcal{A}(d)$ and $f(d)$ calculated for various types of DNA. Upper-left inset shows smoothed $\Delta\mathcal{A}(d)$, reference to global minimum state, for intact nick-free DNA (dark red solid line, 300 K), defected nick-free DNA (dark red dotted line, 300 K), intact nicked DNA (dark blue solid line, 300 K; orange solid line, 290 K), unstacked nicked DNA (dark blue dashed line; 300 K) and peeled nicked DNA (dark blue dotted line, 300 K). Main figure shows continuous $f(d)$ for corresponding types of DNA indicated by correspondingly colored lines. For each type of DNA, force directly read out from the spring indicated by • of corresponding colors are shown for comparison.

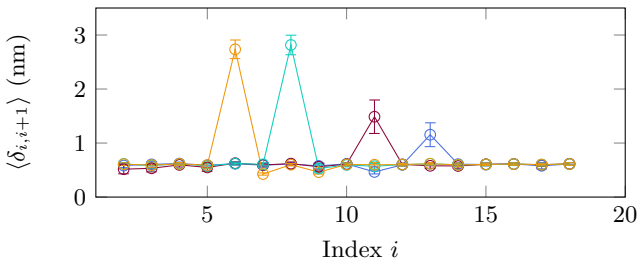

FIG. 5. Basepair distance profiles for nicked DNA. The basepair distance profiles, $\langle \delta_{i,i+1} \rangle$, which measure the equilibrated distances between adjacent C4' atoms of i^{th} and $(i+1)^{\text{th}}$ basepairs on top strand scanned through entire DNA, for simulations with nick right after the 6^{th}, 8^{th}, 11^{th} and 13^{th} basepair steps. The dramatic increased $\langle \delta_{i,i+1} \rangle$ in corresponding nick-containing simulations reveal that the disruptions of basepair occurred at nicked sites. Note that C4' atoms of deoxyriboses are part of the DNA backbone.

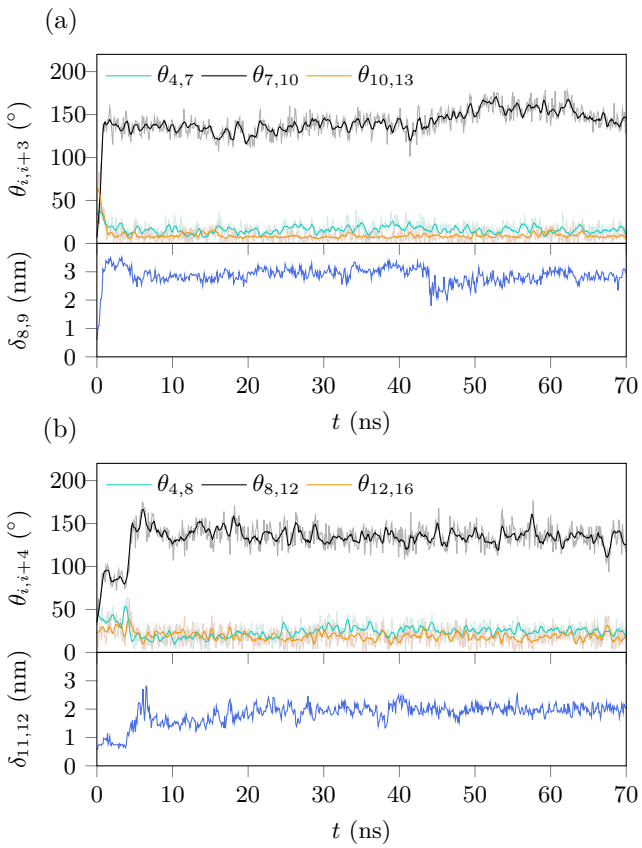

FIG. 6. 70 ns dynamics of local bending deformations and basepair separations at nicked sites under $\kappa = 28.2$ pN/nm. (a) Row 1: time evolution of $\theta_{7,10}$ (black) enclosing nicked site between 8^{th} and 9^{th} basepairs, which shows the kink development around unstacked region. The bending angle evolutions of two intact regions with same length, $\theta_{4,7}$ (cyan) and $\theta_{10,13}$ (orange), are shown for comparison. Rows 2: time evolutions of $\delta_{8,9}$ (dark blue) indicates basepair separation at nicked sites. (b) Similar dynamics of kink development ($\theta_{8,12}$, black), bending relaxation ($\theta_{4,8}$, cyan; $\theta_{12,16}$, orange) and basepair separation ($\delta_{11,12}$, dark blue) for the peeled DNA with nick between 11^{th} and 12^{th} basepair.

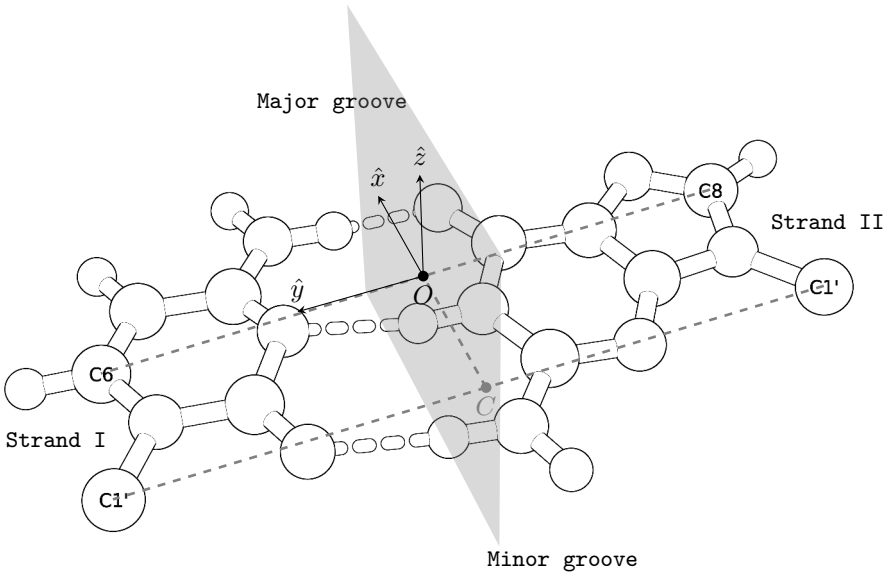

FIG. 7. Basepair reference frame. Reference frame for ideal Watson-Crick basepair using C≡G basepair as example, and only complementary bases are shown. The coordinate is defined by four atoms, C1', C6 from pyrimidine nucleotides (C and T), and C1', C8 from purine nucleotides (G and A). The gray plane, which is the perpendicular bisector of the line segment $\overline{(\text{C1' C1'})}$ at the midpoint C, intersects with the line segment $\overline{(\text{C6 C8})}$ at O. x-axis directs from C to O. y-axis is parallel to $\overline{(\text{C1' C1'})}$, pointing towards the Strand I.z-axis is $\hat{z} = \hat{x} \times \hat{y}$.

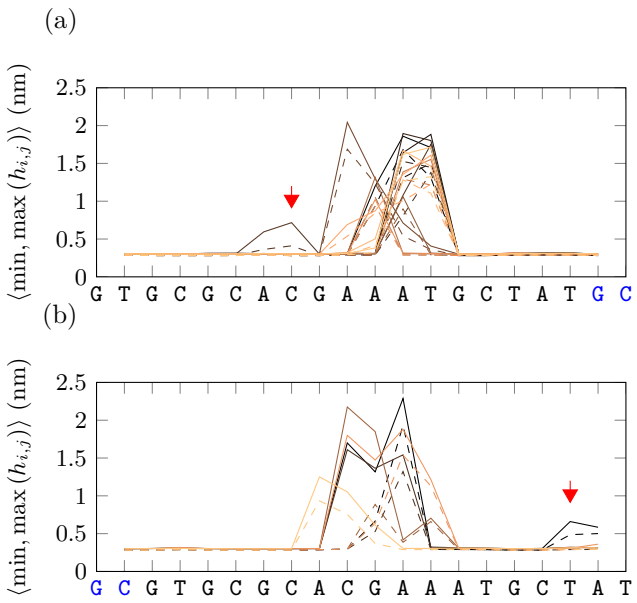

FIG. 8. Central localizations of defects on different sequences. Hydrogen bonding profiles of the defected DNA with original sequence $5' - \texttt{GTGCGCACGAAATGCTATGC} - 3'$ and modified sequence $5' - \texttt{GCGTGCGCACGAAATGCTAT} - 3'$. Overlay of $\langle \min(h_{i,j}) \rangle$ (dashed) and $\langle \max(h_{i,j}) \rangle$ (solid) along the DNA sequence, averaged over the last 20 ns for (a) twelve independent simulations with the original sequence and (b) five independent simulations with the modified sequence, under various bending constraints with $\kappa > 25.0$ pN/nm. These hydrogen bonding profiles were colored from light to dark copper as κ increases, respectively (*i.e.*, $\kappa = 26.6, 28.2_{\mathrm{I}}, 28.2_{\mathrm{II}}, 28.2_{\mathrm{III}}, 28.2_{\mathrm{IV}}, 28.2_{\mathrm{V}}, 29.0, 31.5, 33.2, 41.5, 49.8, 83.0$ pN/nm for original sequence, while $\kappa = 28.2, 31.5, 33.2, 41.5, 49.8$ pN/nm for modified sequence). The modified sequence was generated from the original sequence by removing its tailing $5' - \texttt{GC} - 3'$ and plugging it back to its front, which offset the AT-rich region (*i.e.*, its $10^{\mathrm{th}} - 13^{\mathrm{th}}$ basepairs) away from its center. The arrow in panel (a) indicates an additional disrupted region slightly off center in one of the twelve simulations, while the arrow in panel (b) points out the AT end peeling in one of the five simulations.

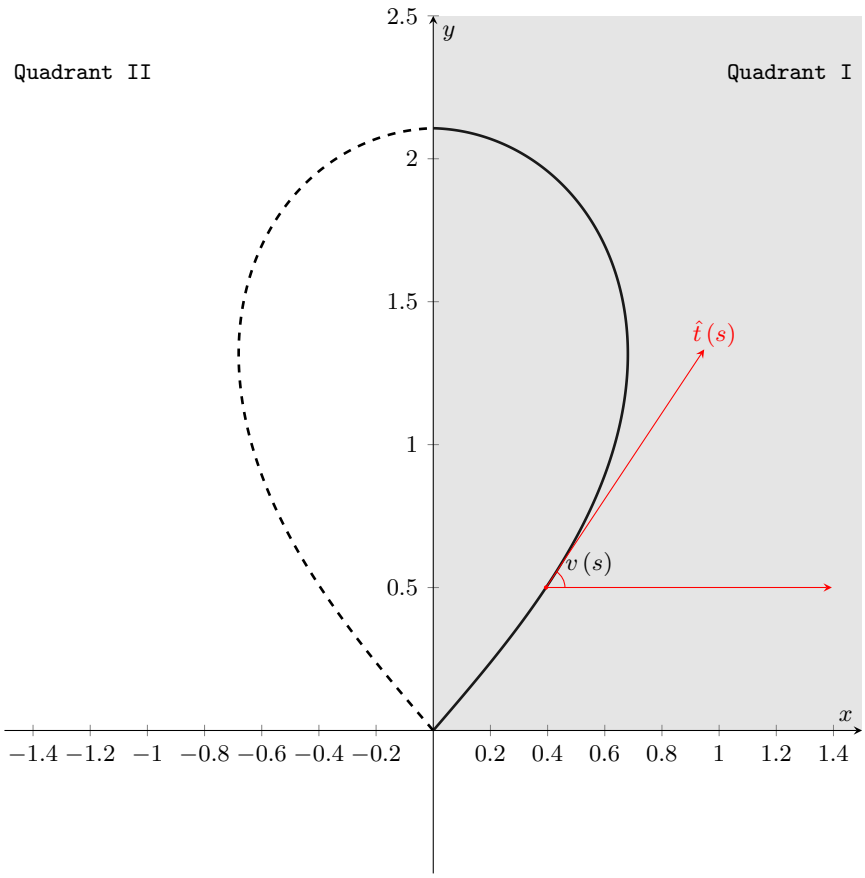

FIG. 9. Energy minimal rigid path of short DNA fragment. A planar looped rigid homogeneous polymer under free boundary condition forms a symmetric path ignoring thermal fluctuations. The energy minimal conformation assumes a teardrop shape (as shown above) [49], which satisfies equation C1 that implies maximized curvature at its center. In the figure above, the contour length is set to be our 20 bp dsDNA simulated length $L = 5.43$ nm, whose two termini make an angle of $\theta = 81°24'$ in the teardrop shape.

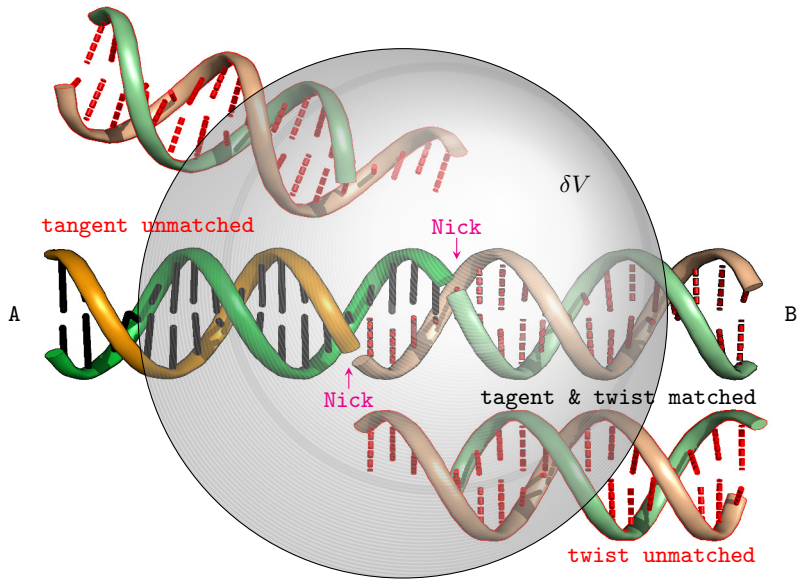

FIG. 10. Ω boundary condition. In ligase based DNA looping experiments, within the infinitesimal volume, δV, around reference "A" end (with black solid basepairing), only a subset of entered complimentary "B" ends (with red dashed basepairing) can assemble into transiently stabilized hybridized "A-B" ends, and chemically trapped by a subsequent ligation reaction. Under the Ω boundary condition defined in the main text, it entails a $(4\pi \times 2\pi)^{-1}$ factor. Tangent unmatched (at top) and twist unmatched (at bottom) "B" ends are shown for comparison. Note that two pre-existing nicks (magenta arrows) are formed right after hybridization, which may cause violation of Ω boundary condition when DNA is sharply bent.

Supplemental Material for: Revisit the anomalous bending elasticity of sharply bent DNA

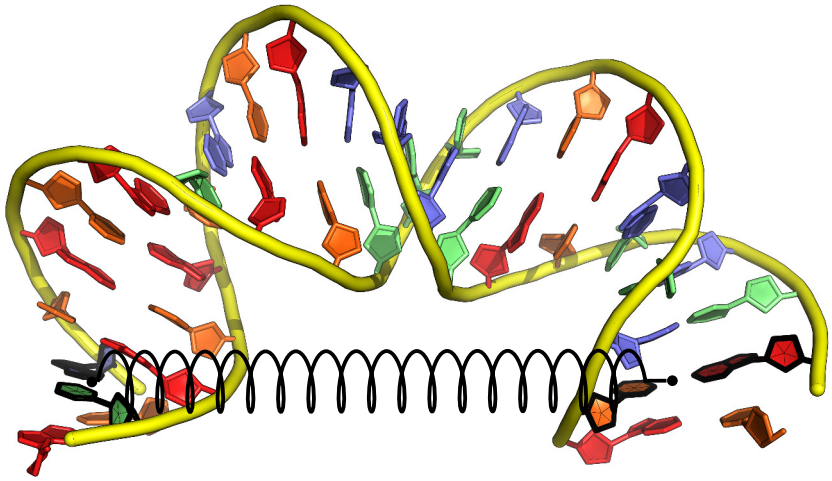

FIG. 1. Initial smoothly bent DNA conformation generated by `X3DNA`. This initial conformation has an overall bending angle of $\sim 160°$. A zero-length spring is connected to the bases of second and second-last basepairs (highlighted by black outlines) to actively pull the DNA ends inward. Note that the nucleotides are colored by sequence, `A` in blue, `T` in green, `G` in red and `C` in orange, while backbones are colored in yellow.

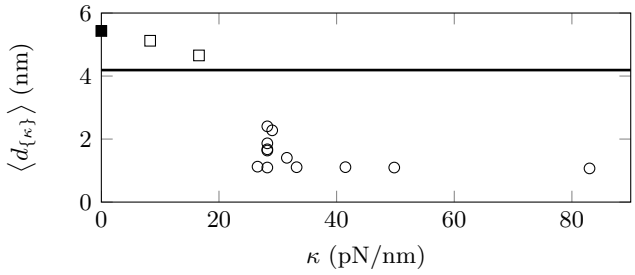

FIG. 2. Mean end-to-end distances $\langle d_{\{\kappa\}} \rangle$ under various κ constrained simulations. They are averaged over last 20 ns for each simulation. $\langle d_{\{0\}} \rangle$ from the unconstrained simulation (■) is shown as control. $\langle d_{\{\kappa\}} \rangle$ with $\kappa < 20.0$ pN/nm (□) are longer than d_{ini} (black line), shorted than control, and negatively correlated with κ. $\langle d_{\{\kappa\}} \rangle$ with $\kappa > 25.0$ pN/nm (○) are much shorter than d_{ini} and uncorrelated with κ.

(a)

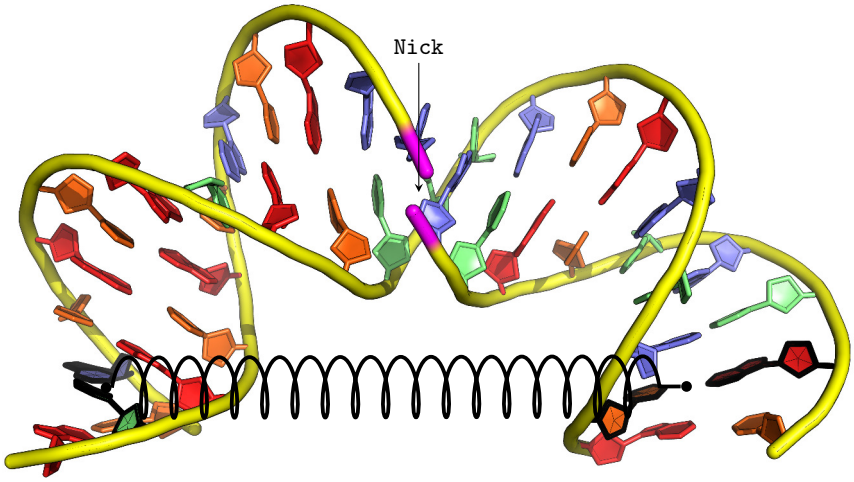

(b)

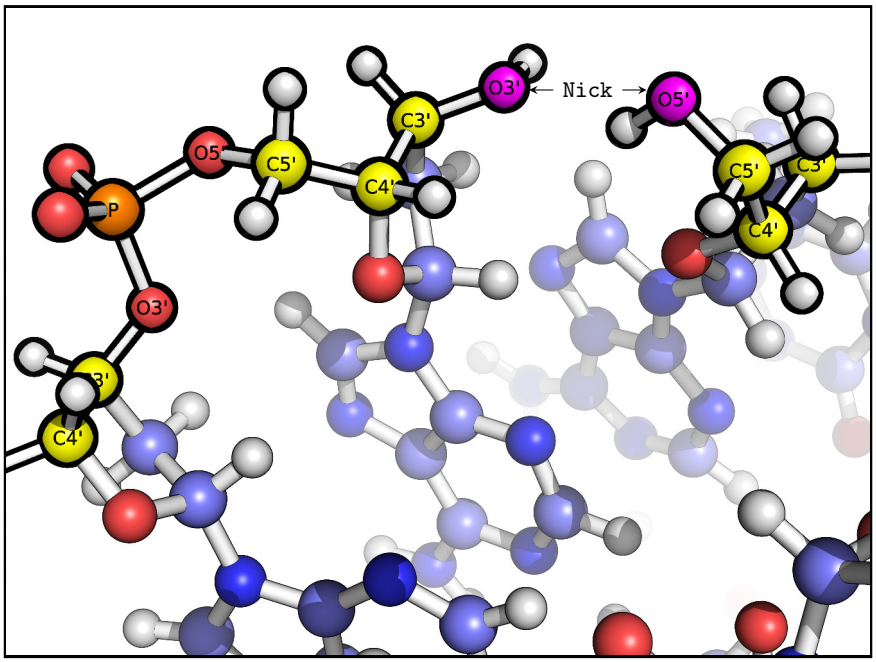

FIG. 3. Nicked DNA constructs with nick after 11th basepair. (a) An smoothly bent DNA initial containing a nick between 11th and 12th basepairs in Strand I, highlighted by magenta. (b) Zoom in at the nicked site, where the phosphate ester bonds were cleaved and entire phosphate group was removed, leaving the O3' and O5' atoms (magenta) hydrolyzed. The backbone carbon atoms are colored by yellow, phosphate atoms are colored by orange and oxygen atoms are colored by red.

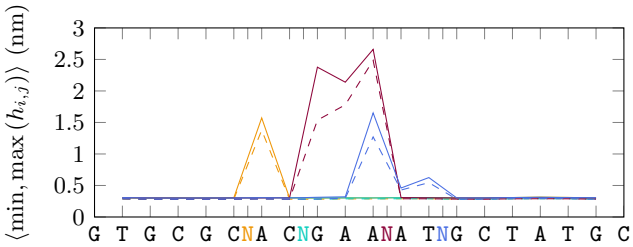

FIG. 4. Hydrogen bonding profiles for nicked DNA. The hydrogen bonding profile, $\langle \min, \max(h_{i,j}) \rangle$ *v.s.* $i = 2, 3, \cdots, 19$ averaged over the last 20 out of 70 ns trajectories for four independent simulations with nick right after the 6^{th}, 8^{th}, 11^{th} and 13^{th} basepair steps. Although their C4' basepair distance profiles in main text already indicated the presences of base-stacking disruptions at nicked sites, these hydrogen bonding profiles further reveal the existence of two distinctive types of disruptions: clean unstacking at nicked site (*i.e.*, with intact hydrogen bonding) in the case of nick after 8^{th} basepair step, and unstacking accompanied by peeling from nicked sites (*i.e.*, with disrupted hydrogen bonding) in the case of nicks after 6^{th}, 11^{th} and 13^{th} basepair steps.

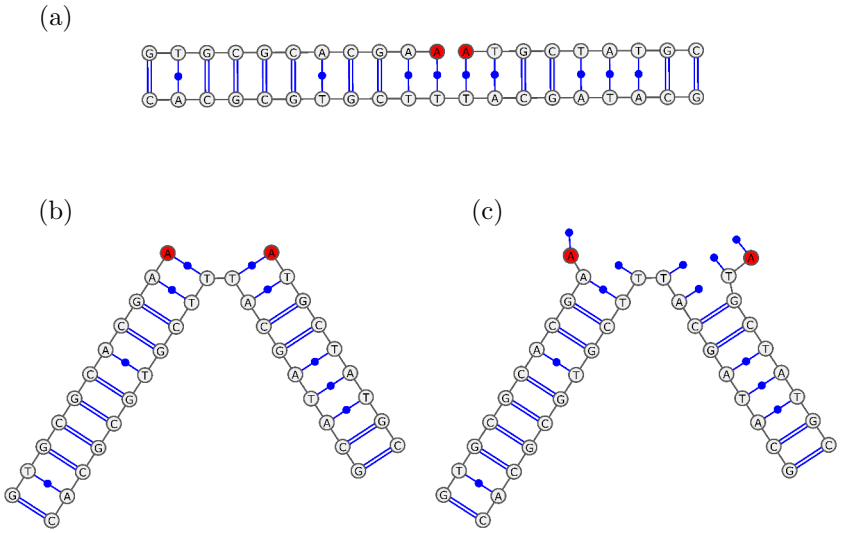

FIG. 5. Illustrations for nicked DNA with different categories of non-covalent topologies. (a) Type A shows the intact nicked DNA with both intact hydrogen bonding and basepair stacking. (b) Type B represents the unstacked nicked DNA with disrupted basepair stacking only at nicked position. (c) Type C indicates a particular case of the peeled nicked DNA with both nicked ends split, resulting in both disrupted base-stackings and base-pairings around nicked site. This figure uses planner structures with nick after 11^{th} basepair as demonstrations.

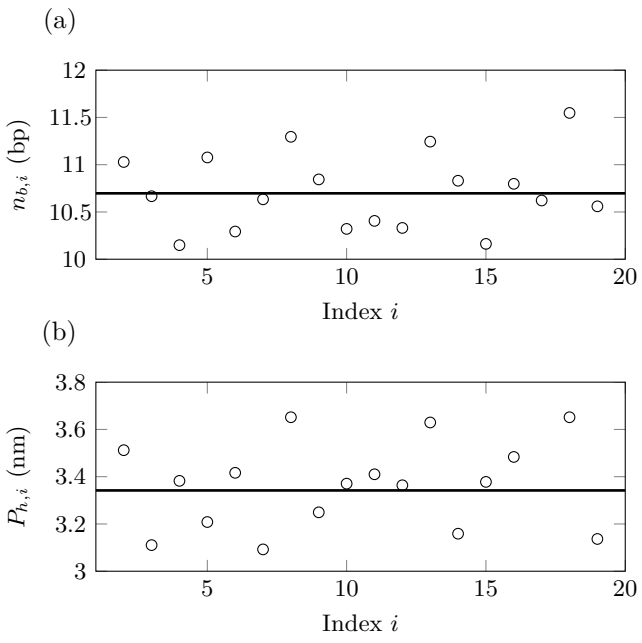

FIG. 6. Helical parameters for B-DNA without constraints. (a) Helical repeat, $n_{b,i}$ and (b) helical pitch, $P_{h,i}$ along DNA are derived using average twist and rise at particular site (i) over the last 20 ns of 70 ns simulation. Black lines show their global mean obtained by $n_b = 2\pi/\langle\Omega\rangle$ and $P_h = 2\pi\langle D_z\rangle/\langle\Omega\rangle$ at 10.70 ± 0.07 bp and 3.34 ± 0.03 nm, respectively, where Ω is twist angle, D_z is rise per basepair step, and the values after $\pm$ sign are corresponding standard errors calculated from uncorrelated structure representatives. $n_{b,i}$ and $P_{h,i}$ are all around their global mean, which indicates the homogeneity of DNA.